BNL--48488

DE93 006671

Strong-Field Dissociation Dynamics

L. F. DiMauro and Baorui Yang
Chemistry Department, Brookhaven National Laboratory, Upton, NY 11973

ABSTRACT

We examine the strong-field dissociation behavior of diatomic molecules under two distinctive physical scenarios. In the first scenario, we discuss the dissociation of the *isolated* hydrogen and deuterium molecular ions. The dynamics of above-threshold dissociation (ATD) are investigated over a wide range of green and infrared intensities and compared to a dressed-state model. The second situation arises when strong-field neutral dissociation is followed by ionization of the atomic fragments. The study results in a direct measure of the atomic fragment's ac-Stark shift by observing the intensity-dependent shifts in the electron or nuclear fragment kinetic energy.

1. INTRODUCTION

Over the last decade studies examining the behavior of isolated atoms in strong radiation fields have resulted in a cumulative literature rich in new phenomena, unresolved issues, and exciting new predictions for future studies.[1] Recently, similar investigations have begun to examine the general behavior of molecules in intense fields, especially in the studies of photodissociation dynamics. The additional challenge associated with studying molecules in strong fields result from the difficulty of sorting out the general behavior of field-induced effects from the details or specifics of the molecular structure. Investigations on atoms[2,3] clearly demonstrate the importance of the atomic structure in describing the ionization dynamics in the multiphoton regime. Consequently, it is not surprising to expect enhanced structural effects in molecules due to the many internal degrees of freedom as compared to atoms. In addition, molecular strong-field studies raise some interesting and unique questions concerning the role and interplay of ionization and dissociation and can result in studies of atoms in unusual circumstances. The fundamental motivation for such studies derives its interest from the ability to control chemical dynamics by external variation of a laser field. The traditional chemical physics approach relied upon the laser frequency as the only external field parameter for achieving state-selectivity but has met with little success. However, current efforts[4] have focused on examining all aspects of the laser field for achieving control. Although premature in realization, an understanding of the influence of intensity, coherence, phase, and pulse duration and shaping in concert with frequency may ultimately lead to our ability or inability to control chemical dynamics.

In this paper, we report on our progress in conducting a systematic investigation on the strong-field dissociation dynamics of diatomic molecules. These studies involve multiphoton excitation in the intensity regime of $10^{11\text{-}14}$ W/cm^2 with the fundamental and second harmonic of a Nd:YAG or Nd:YLF laser system. Measurements include energy resolved electron and mass spectroscopy which provide useful probes in elucidating the interaction dynamics predicted by existing models. The first example examines the strong-field dissociation of H_2^+ and D_2^+ at green (Section 3.1) and infrared (Section 3.2) frequencies. Both diatomic ions are formed via multiphoton ionization of the neutral precursor which is physically separable from the dissociation process. This study provides the first observation of the dynamics associated with the ATD process and analogies will be made with the more familiar above-threshold ionization (ATI) phenomenon. The final investigation (Section 3.3) involves a scenario in which both the dissociation of the molecule and the subsequent ionization of the neutral atomic fragments originate from the same superexcited molecular potential. This study focuses on the effect that the molecule-field interaction has on the redistribution of energy from ponderomotive or ac-Stark shifts among the electrons, the nuclear fragments, and the field. An experimental study of chlorine molecule and fragments will be presented and interpreted within this framework.

2. EXPERIMENTAL

The photon sources used are well characterized Nd:YAG (1.06 μm, 10 nsec, 10 Hz) and Nd:YLF (1.05 μm, 50 psec, 1 kHz) lasers. Details of these laser systems have been described previously.[5] The second harmonic is generated using standard nonlinear techniques either in BBO or KD*P crystals. The intensity ranges for 0.532 and 0.527 μm radiations are 8×10^{11} to

MASTER

DISTRIBUTION OF THIS DOCUMENT IS UNLIMITED

Dimauro

9.7×10^{12} W/cm^2 and 5×10^{12} to 4×10^{13} W/cm^2, respectively. The apparatus consists of an ultrahigh vacuum chamber equipped with time of flight electron and mass spectrometers. The field-free photoelectron spectrometer has an energy resolution of about 50 meV for 1 eV electrons and an acceptance angle of 1×10^{-3} sr. It is calibrated using the well known ATI spectrum of xenon atoms. The mass spectrometer consists of a 42 cm long drift tube with a series of electric field acceleration plates. Fragment kinetic energy analysis is achieved by applying an uniform extraction field across the laser focus with the laser polarization parallel to the flight tube axis. This produces two nearly symmetric peaks in the time of flight spectrum corresponding to the two velocity components of the same fragment initially directed towards and away from the detector. The kinetic energy of the fragment is simply determined by measuring the arrival time difference between the peaks. The mass spectrometer energy calibration was performed by recording the weak-field photodissociation of chlorine[6] molecules. The resolution was estimated to be about 100 meV for 1 eV protons. The background pressure in the ultrahigh vacuum system was 1×10^{-9} torr. The data collection system is always operated in the pulse counting regime with count rates much less than one event per laser shot.

3. RESULTS AND DISCUSSION

A physically distinct motivation for studying the strong-field behavior of molecules instead of atoms is the presence of dissociative channels. Questions addressing the validity of extending our knowledge on intense field atomic ionization to describe molecular dissociation seem warranted. For example, does high field dissociation proceed in an analogous manner to ATI, that is, via absorption of additional photons beyond the minimum needed to break a molecular bond and are the dynamics similar. Molecular hydrogen represents the *"model"* system to address these issues because of its simple and well-known structure and as a result should provide the foundations for future molecule-field studies. Furthermore, as we will see in section 3.3, the atoms formed via the dissociation process present the possibility to probe their behavior in a physically different environment as compared to the more common isolated atom experiment.

3.1. H_2^+ dissociation: 0.53 μm excitation

The intense laser field photodissociation of H_2^+ has been described by the mechanism of bond-softening[7,8] using a dressed molecular state formalism. In this model, the laser field is considered as a strong perturber to the molecular potential. The potential curves couple and distort via the strong dipole interaction. Since the ground ionic state and the first repulsive state have symmetry $^2\Sigma_g^+(1s\sigma_g)$ and $^2\Sigma_u^+(2p\sigma_u)$ respectively, only 1, 3, 5, ... (odd number) photons can be used to dress the transition state because of parity conservation. However, a *net even number* of photon dissociation can also occur due to the absorption and stimulated emission of photons. Intense fields cause the laser induced avoided crossing gap to open up. Any ions with vibrational energy within the gap should become unstable. As the laser intensity is increased and the molecular potentials distort, one should observe a negative shift in the proton kinetic energy corresponding to dissociation from the lower vibrational states of H_2^+. Furthermore, the absorption of more photons ($N \geq 2$) from the same vibrational states results in a series of peaks separated by about a photon (total) kinetic energy (ATD). Likewise, the distorted potentials result in a change in the vibrational energy eigenvalues resulting in a positive shift in the photoelectron spectrum.

Figure 1 shows a typical time of flight mass spectrum resulting from the 0.532 μm nonresonant MPI of H_2 and D_2 molecules at an intensity of 9.7×10^{12} W/cm^2. The molecular ions formed by the MPI of the neutral molecule produces the peak at long arrival times in the spectra of Fig. 1. The peaks at the short arrival times are the atomic fragments (protons and deuterons) formed via dissociation of the molecular ion. The symmetric substructure results from the forward and backward directed fragments and the splitting is proportional to their initial kinetic energy, as discussed in Sec. 2. The three fragment peaks are labeled according to the number of photons being absorbed by molecular ions leading to dissociation. According to our experimental results at low intensity most H_2^+ ions are dissociated from the $v^+_{avg} = 5$ vibrational level following the absorption of a single photon (peak 1 in Fig. 1). The maximum of this peak is observed to shift from $v^+ = 5$ to $v^+ = 4$ at higher intensities. With increasing intensity another peak emerges corresponding to two photon (peak 2 in Fig. 1) dissociation via $v^+_{avg} = 2$. Consequently its separation is less than a photon total energy from the first peak due to differing initial vibrational states and is intensity dependent. At still higher intensities a third peak appears about one photon total energy away from the second peak corresponding to a three photon dissociation. The same general behavior is observed for D_2 and HD molecules. Similar kinetic energy shifts are observed in the 0.527 μm (psec) spectra over an intensity range of 5×10^{12} to 4×10^{13} W/cm^2. Shown in Fig. 2(b) is the dissociation fraction F^H and F^D as a function of laser intensity for H_2^+ and D_2^+, respectively and where $F^H = [H^+/(H^+ + H_2^+)]$ and $F^D = [D^+/(D^+ + D_2^+)]$. Note, that the dissociation fraction for each molecule increases with intensity and that F^D is larger than F^H at all intensities shown.

We have carefully examined the photodissociation of H_2^+ molecules by recording the proton kinetic energy spectra and the H_2 photoelectron spectra simultaneously as a function of laser intentisy. Our results verify that the mechanism responsible for H^+ and D^+ formation is the photodissociation of the parent molecular ion. It appears that the amount of H^+ produced is proportional to that of photoelectrons due to (7+1) molecular ionization. In addition, energy conservation implies that seven second harmonic photons of YAG(YLF) can populate only up to $v^+ = 3(4)$ vibrational levels in the ionic ground state, whereas the lowest intensity data have proton energies peaked at $v^+ = 5$. Thus, we conclude that the H^+ peak labeled 1 in Fig. 1 (0.7 eV total energy) is due to the eight photon ionization of H_2 followed by one photon dissociation of H_2^+.

Our results are generally in qualitative agreement with the bond-softening model but there remain some quantitative differences. In the current experiment, we observed apparent negative shifts in proton kinetic energies with increasing laser intensity with both 532 nm (ns) and 527 nm (ps) pulses. The maximum population of the 1-photon proton kinetic energy peak shifts by ~ 200 meV over the entire intensity range. Likewise, the maximum of the ionic vibrational state distribution in the photoelectron spectroscopy (PES) changes from high to low vibrational levels in a similar intensity range, although the shift in the amplitude of the vibrational distributions is independent of the molecule studied. Thus, the bond--softening mechanism to first order is predominantly an electronic coupling and not vibrational. However, we could not observe any commensurate positive energy shifts in the PES peak positions with increasing intensity although a broadening is clearly evident. An asymmetric broadening in our PES could result from spatial or temporal averaging in our experiment masking a "pure" energy shift but the sign of the observed broadening is opposite to that predicted by a bond-softening model.[7] This inconsistency could imply a shortcoming in our numerical method or an indication that the PES probes the potential at a low intensity before significant potential distortion has occurred. Another contributing factor to the peak width could result via strong-field rotational pumping with increasing laser intensity, causing the photoelectron peaks to broaden towards lower energies.

Referring to Fig. 2(a), the ratio (R_{21}) of dissociation via 2-photon versus the 1-photon channels (peaks labeled 1 and 2 in Fig. 1) for H_2^+ changes from 7% to 25% as the intensity is increased to 9.7×10^{12} W/cm^2. Furthermore, the ratio R_{32} for 3 versus 2-photon dissociation decreases from 16.5 to 6.5% in the same range. Interestingly, the behavior in D_2^+ is somewhat different, here the fraction R_{21} changes from 17 to 40% which is larger than H_2^+. However, the D_2^+ ratio R_{32} is smaller than H_2^+ and relatively constant (~ 6%) over the entire intensity range. These branching ratio effects can be all understood with the same model.[8] Physically, the increasing laser intensity corresponds to a larger avoided-crossing gap resulting in a decrease in the 3-photon diabatic transition rate while favoring 2-photon adiabatic passage (3-photon absorption, 1-photon emission). Since H_2^+ and D_2^+ have a relatively large difference in vibrational frequencies due to their different masses, therefore at low intensities where the gap is not large enough to completely shut off the 3-photon diabatic path as compared to H_2^+ due to the fact that a smaller vibrational frequency implies more adiabatic motion. Specifically, $R_{32}(H) > R_{32}(D)$ at low intensity. As the gap continues to widen, one should also observe the ratio R_{32} to decrease for both H_2^+ and D_2^+ molecules. Such behavior is clearly demonstrated in our experiments. Figure 2(a) also shows for comparison the results of the calculated fragment R_{32}^{LZ} ratios predicted by a simple Landau-Zener (LZ) theory.[10] The theory predicts well the general behavior of the ratios as the light intensity changes. However, the calculated ratios are approximately three times larger than the experimental values which could imply that the degree of deformation of the calculated potential curves is beyond the limits of applicability of simple LZ theory.

3.2. H_2^+ dissociation: 1.06 μm excitation

Figure 3 is a plot of a typical time of flight mass spectrum resulting from dissociation of H_2 with 1.06 μm radiation. The dissociation fraction F^H for H_2^+ molecules, where $F^H = [H^+/(H^+ + H_2^+)]$, changes from 0.25 to 0.43 for the entire dynamic range of laser intensities 2.3 - 4.6 x 10^{12} W/cm^2. The peaks labelled *a* and *b* correspond to a total proton kinetic energy of 0.49 and 2.88 eV, respectively, and are assignable to the dissociation of H_2^+ following absorption of 2- and 4-photons. For both processes, the measured proton kinetic energies give an initial vibrational distribution with an average value of $v_{avg} = 3$. No odd number photon dissociation processes are observed in the present experiment at all intensities studied. Furthermore, the ATD ratio, $R_{42}(H)$, for the 4-photon and 2-photon dissociation channels are intensity dependent and increase from 0.11 to 0.14 with increasing intensity.

The photoelectron spectra of H_2 taken at two different laser intensities with 1.06 μm radiation is shown in Fig. 4. The tick marks indicate the number (order) of photons absorbed by the H_2 molecule. Since the IP of H_2 is 15.42 eV, a minimum of 14 photons are required to ionize. The low-intensity photoelectron spectrum plotted in Fig. 4(b) can be characterized as a broad distribution centered at 5 eV which exhibits suppression of low energy electrons up to 2.8 eV and a maximum kinetic

energy at 15 eV. However, the spectrum still shows structure which is vibrationally resolvable and assignable to the first four vibrational levels of the H_2^+ ground state. As the laser intensity is increased in Fig. 4(a), the photoelectron distribution tends to become structureless and shifted towards higher kinetic energy (peaked at 7.5 eV). Likewise, the low-energy electron peaks associated with the 16 and 17-photon ionization processes show additional suppression. The MPI and dissociation of H_2 at 1.06 μm have been studied by Zavriyev *et al.*[7] using 100 ps pulses. Their photoelectron distributions show a similar shape to those shown in Fig. 4 but with no resolvable structure. The difference between the two experiments probably reflects the change in saturation intensity *via* the pulse width dynamics which unfortunately results in an inability to extract any detailed information from the photoelectron spectrum. Consequently, long pulse studies can provide a better mapping of the molecule-field interaction. The mechanism resulting in the suppression of low energy electrons in Fig. 4 is not understood. The suppression is analogous in its behavior to *"channel closure"* observed in rare gas atoms[11] which is caused by the increasing binding energy of the atom in the field and proportional to the ponderomotive potential. However, the pondermotive potential available at our highest intensity is only 0.5 eV, which is obviously not enough shift to account for our degree of electron suppression.

The proton kinetic energy spectrum of Fig. 3 shows no evidence that 1-photon dissociation is occurring at 1 μm. Thus, bond-softening is not playing any significant role in the dissociation dynamics at this wavelength, although it dominates at 0.53 μm. This result is not difficult to understand, since the 1-photon curve crossing associated with the dressed-state picture illustrated in Fig. 5, occurs at large enough internuclear separation (~ 5 bohr) which necessitates the need for significant population in the higher vibrational (v = 7) levels of the molecule. However, our photoelectron spectrum analysis shows that only the lower vibrational states are populated via the MPI process.

As discussed above for 0.53 μm excitation, the ATD ratio (R_{32}) decreases with increasing laser intensity, that is, dissociation occurs more readily through the lower-order channels as the laser intensity increases. This behavior is just the opposite at 1 μm, where the ATD ratio (R_{42}) increases with rising intensity. The 1 μm behavior is analogous to the more familiar intensity dependence observed in ATI. Although this strong wavelength dependence results in such different dynamics, the interpretation is all consistent with the dressed-state model discussed above. According to the dressed-molecular states model, illustrated in Fig. 5 for 1 μm radiation, the diabatic dressed-states $|u,3>$ and $|u,5>$ cross the ground state $|g,0>$ at 3.6 and 3.1 bohr, respectively. Furthermore, the intersections are electric-dipole allowed ($g \rightarrow u$) which result in an intensity-dependent avoid-crossing. The gap also occurs in the potential region which are vibrational populated by the MPI process. The same argument applies to the diabatic crossing (dashed line in Fig. 5) between the $|g,2>$ and $|u,3>$ curves. The 1-photon interaction results in an avoid-crossing which is more strongly laser dependent than the higher order processes. Consequently, the high intensity and longer wavelength causes the 1-photon gap to become so large (solid lines) that adiabatic passage dominates (3-photon absorption, 1-photon emission) resulting in only 2-photon dissociation. The same logic then follows for any dressed-state pairs, *i.e.* $|g,4>$ and $|u,5>$, which always result in even-photon dissociation. This is physically manifested in our proton kinetic energy spectrum as the series of peaks separated by the 2-photon (total) energy. Likewise, the increase in the ATD ratio (R_{42}) results from the fact that each proton peak in the series occurs via a different order photon process. Thus, the dynamics, as manifested by the increasing ATD ratio, results in more efficient production of higher-order protons with increasing intensity. This has similar dynamics compared with production of high energy ATI electrons.

3.3. Laser-induced shifts in nuclear fragments

It is well understood that under proper laser pulse conditions, atomic energy levels and ionization potentials (IP) shift.[11] Except for very short pulses,[2] these changes are usually not directly measurable due to the energy gained by the freed electron as it slides down the laser field gradient via ponderomotive acceleration. The shift of energy levels resulted in similar effects in the case of molecular ionization.[12] Moreover, if a molecule can dissociate through one of these states, this same shift would also influence the kinetic energy of the dissociating fragments.[13] In this section we will describe a study on chlorine molecules with 0.53 *μm* radiation where such a situation occurs and measurable as a light-induced shift in the kinetic energy of nuclear fragments. This investigation differs from the H_2^+ study discussed above which treats ionization and dissociation processes separately.

In our experiment, excited Cl atoms are prepared by the five photon (0.53 *μm*) excitation of Cl_2 above the ionization limit, as shown in Fig. 6. At this point the super-excited $[Cl_2]^*$ molecules can ionize or dissociate with similar rates[14] due to the details of continuum structure. Direct neutral dissociation occurs via the $3^3\Pi_u$ Rydberg state which has been identified[14] to

converge onto the A $^2\Pi_u$ ionic state, producing chlorine atoms in the ground and the excited ^4P_J ($3s^23p^44s$) states. Once the ^4P_J state of Cl atom is formed, it can subsequently ionize producing a photoelectron.

Figure 7 shows photoelectron spectrum of Cl_2 at 3×10^{12} w/cm^2. The molecular ions which are formed via five photon ionization dominate the total population (lowest energy peaks). The six photon and higher order ATI of Cl_2 are observed with relatively lower magnitude. At the highest intensities (not shown), the electron spectrum shows a series of peaks assignable to the six photon ionization and associated ATI of ground state atomic chlorine. Details of these molecular transitions will be discussed in a future paper. The most interesting part of the spectrum however, are the relative amplitudes and positions of the peaks at 0.77, 3.13 and 5.49 eV, originating from the two, three, and four photon ionizations of the excited state (^4P_J) Cl atoms. These peaks are observed to be shifted towards higher energies and the magnitude of shifts vary approximately linearly with laser intensity, as shown for the lowest energy peak (open circle) in Fig. 8.

We have also examined the energy resolved Cl fragment spectrum (not shown) and it gives a commensurate result with our photoelectron assignment. *The total Cl fragment kinetic energy was also observed to shift with increasing intensity but towards lower energies*, as shown by the solid circles in Fig. 8 (note that the left and right ordinate axes have opposite signs). However, due to the lower resolution of the mass spectrometer the measured uncertainty is larger compared to the electron data. After careful examination, we are unable to assign any other transitions that will result in electrons and ions with the observed energy distributions, except for the (^4P_J) excited state of Cl atom. In addition, we have also systematically eliminated the possibility of space charge and contact potentials as sources of this shift. Above all, other peaks in the spectra are not affected by these shifts. We should mention that at our final state energy, an assignment consistent with ours has been made by Koenders *et al.*[14] in their (2+1) resonance enhanced MPI and PES studies of chlorine molecules.

In essence, since the laser intensity required for a five photon process is substantial, the outermost electron of the molecule starts wiggling with the laser field. As a result, the molecular potential and the dissociation threshold are shifted by similar amount as the two atoms separate from each other, as shown by dashed curves in Fig. 8. The total kinetic energy of the dissociation fragments at the point of creation is shifted and given by

$$KE = n\hbar\omega - (E_{4_P} + D_0^0) - U_{ac}^e \qquad (1)$$

where D_0^0 is the ground state dissociation energy of Cl_2, E_{4_P} is the energy of the ^4P Cl atom, U_{ac}^e is the ac-Stark shift of the electron in the ^4P Cl atom, and n is the number of photons needed to populate the dissociative molecular state ($3^3\Pi_u$ for our case). Here we assume that the wiggling of the nuclei is negligible. Note, that the mechanism presented here for chlorine can be generalized for any case. As shown in Fig. 8, the neutral $3^3\Pi_u$ and ionic $X^2\Pi_g$ states have been shifted by U_{ac}^e and the ponderomotive potential U_p^e, respectively. Once the molecule dissociates and the atoms start to absorb more photons, the situation becomes completely different from one in which the excitation is from an unshifted ground state. For excited atoms which are formed in intense fields, the photoelectron kinetic energy at the point of creation is

$$KE_e = m\hbar\omega - (IP - E_{4_P}) + U_{ac}^e - U_p^e \qquad (2)$$

where m is the number of photons required to ionize the excited fragments (note: $m < n$). If we assume that both initial and final states have shifted by the same amount ($U_{ac}^e = U_p^e$), the situation will be exactly same as the field free ionization where the electron kinetic energy is $KE_e = m\hbar\omega - (IP - E_{4_P})$. Thus, the electron kinetic energy at creation is *independent* of the laser intensity. This is also the measured kinetic energy when the laser pulse width is in the short pulse regime. However, in our long-pulse experiment, the measured kinetic energy will be

$$KE_e^{det} = m\hbar\omega - (IP - E_{4_P}) + U_{ac}^e \qquad (3)$$

which is increased by the amount U_{ac}^e and is *intensity dependent*. Furthermore, the increase (decrease) in the kinetic energy of the electron (Cl fragment) is a direct measure of the ac-Stark shift of the excited state. Figure 8 shows the measured kinetic energy shifts for electrons (open circles) and ^4P Cl atoms (solid circles) as a function of laser intensity for 527 nm radiation. Note, that the electron and atomic fragment shifts are equal in magnitude but opposite in sign, consistent with Eqns. (1) and (3). The solid line indicates the detected kinetic energy assuming a pure ponderomotive shift U_p^e and the dashed line is the

DI MAURO

calculated ac-Stark shift of the ^4P state using single-channel quantum-defect theory (SQDT). The large ac-Stark shift for the ^4P_J state, which is approximately equal to U_p^e, is due to the strong couplings at these frequencies to the 4p states. Note, that the measured shifts are linear with laser-intensity and thus consistent with the lowest order perturbation theory scaling.

The physical process proceeds as follows; ground state Cl_2 is promoted to a super-excited state $[Cl_2]^*$ via 5-photon absorption with its outer electron wiggling proportional to the field. The $[Cl_2]^*$ can autoionize or dissociate. Dynamically, as the two atoms separate the wiggling electron finds itself on the excited ^4P atomic fragment. Thus, the additional electron energy U_{ac}^e results in a loss in the fragments' kinetic energy of an equal amount. Subsequent ionization of the ^4P fragment proceeds in an unperturbed (field-free) manner since the field energy U_{ac}^e is already incorporated into the ^4P electron. Some immediate consequences of this scenario are as follows. (1) Information concerning the field-atom interaction can be extracted from the kinetic energy analysis of either fragment (ground or excited), at any time after the intense pulse, regardless of the pulse's temporal regime [Eq. (1) is always valid]. (2) Interpretation of this model predicts an ability to suppress lowest-order dissociation channels in a manner directly analogous to suppression of ionization. Even more subtle, is the capability to dramatically alter the dissociation cross-section via dynamical shifts of repulsive potentials.

4. CONCLUSIONS

In conclusion, the experiments presented above clearly demonstrate the effectiveness that an external field has in altering the dissociation dynamics. Furthermore, the dress-state picture has proven to be a potent intuitive model for understanding the high-field dynamics and should provide a valuable predictive model for future studies. We have also studied in chlorine an universal situation for strong-field dissociation affecting the redistribution of energy from ponderomotive/ac-Stark shifts among the electrons, fragments, and field.

5. ACKNOWLEDGEMENTS

We would like to thank Dr. Xian Tang for his useful discussions on the chlorine work and use of his SQDT calculations. This research was carried out at Brookhaven National Laboratory under contract No. DE-AC02-76CH00016 with the U.S. Department of Energy and supported by its Division of Chemical Sciences, Office of Basic Energy Sciences.

6. REFERENCES

1. See for example, *Atoms in Intense Fields*, edited by M. Gavrila (Academic Press, Orlando, 1992).
2. R. R. Freeman, P. H. Bucksbaum, H. Milchberg, S. Darak, D. Schumacher, and M. E. Geusic, *Phys. Rev. Lett.* **59**, 1092 (1987).
3. Dalwoo Kim, S. Fournier, M. Saeed, and L. F. DiMauro, *Phys. Rev.* **A41**, 4966 (1990).
4. See for example, *Coherence Phenomena in Atoms and Molecules in Laser Fields*, ecited by A. D. Bandrauk and S. C. Wallace (Plenum Press, New York, 1992).
5. M. Saeed, D. Kim, and L. F. DiMauro, *Appl. Opt.* **29**, 1752 (1990); L. F. DiMauro, D. Kim, M. W. Courtney, and M. Anselment, *Phys. Rev.* **A38**, 2338 (1988).
6. L. Li, R. Lippert, J. Lobue, W. Chupka, and S. Colson, *Chem. Phys. Lett.* **151**, 335 (1988).
7. A. Zavriyev, P. Bucksbaum, H. Muller, and D. Schumacher, *Phys. Rev.* **A42**, 5500 (1990); B. Yang, M. Saeed, L. F. DiMauro, A. Zavriyev, and P. Bucksbaum, *Phys. Rev.* **A44**, R1458 (1991).
8. A. Bandrauk and M. Sink, *J. Chem. Phys.* **74**, 1110 (1981); A. Guisti-Suzor, X. He, O. Atabek, and F. Mies, *Phys. Rev. Lett.* **64**, 515 (1990); M. V. Fedorov, O. V. Kudrevatova, V. P. Makarov, and A. A. Samokhin, *Opt. Comm.* 13,2991975).
9. D. T. Strickland, Y. Beaudoin, P. Dietrich, and P. B. Corkum, *Phys. Rev. Lett. 68*, 2755 (1992).
10. L. D. [illegible]ndau, and E. M. Lifshitz, *Quantum Mechanics* (Pergamon Press, New York, 1965).
11. R. R. Freeman, P. H. Bucksbaum, and T. J. McIlrath, *IEEE J. Quant. Elec.* **24**, 1461 (1988).
12. H. Helm, M. J. Dyer, and H. Bissantz, *Phys. Rev. Lett.* **67**, 1234 (1991); G. N. Gibson, R. R. Freeman, and T. J. McIlrath, *Phys. Rev. Lett.* **67**, 1230 (1991).
13. M. Saeed, B. Yang, X. Tang, and L. F. DiMauro, *Phys. Rev. Lett.* **68**, 3519 (1992).
14. B. Koenders, S. Koeckhoven, G. Kuik, K. Drabe, and C. de Lange, *J. Chem. Phys.* **91**, 6042 (1989); S. D. Peyerimhoff and R. J. Buenker, *Chem. Phys.* **57**, 279 (1981).

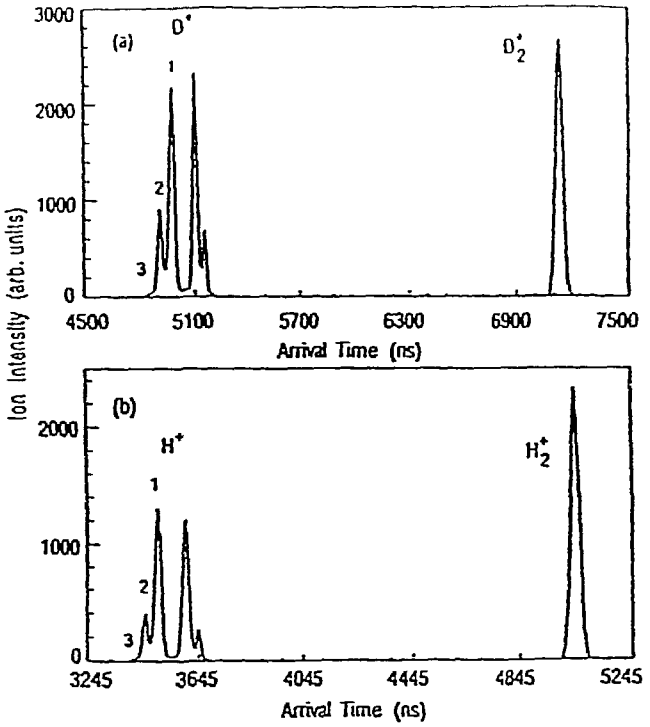

Figure 1: Time-of-flight mass spectrum resulting from 0.53 μm MPI dissociation of (a) D_2 and (b) H_2 at 9.7×10^{12} W/cm^2. Peaks labelled 1, 2, 3 indicate the number of photons absorbed in dissociation. The laser polarization is parallel to the flight tube's axis. An extraction field of 17 V/cm is used in the current experiment.

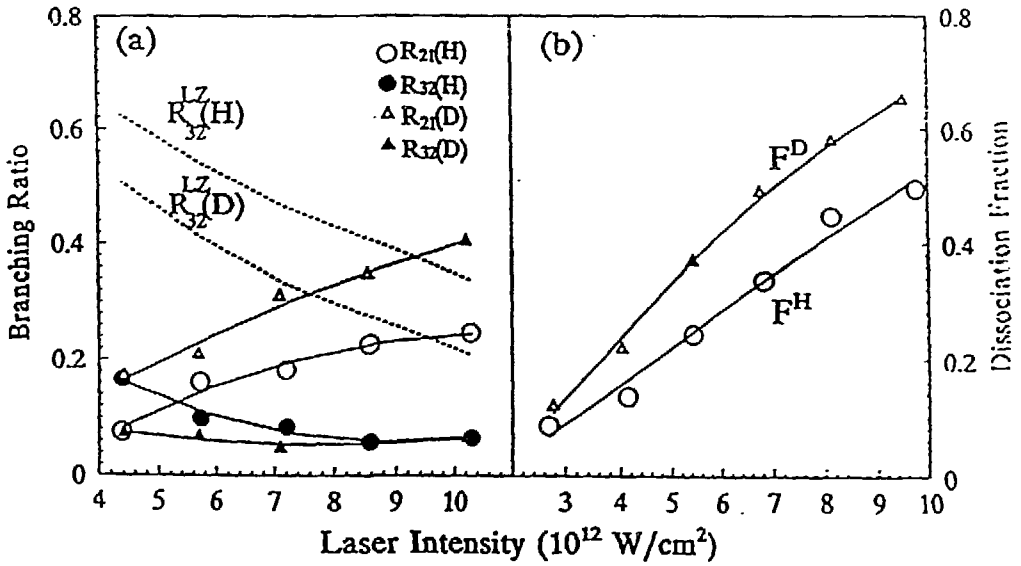

Figure 2: A plot of the (a) ATD branching ratios, R, and (b) dissociation fraction, F, for H_2 and D_2 as a function of 0.53 μm intensity.

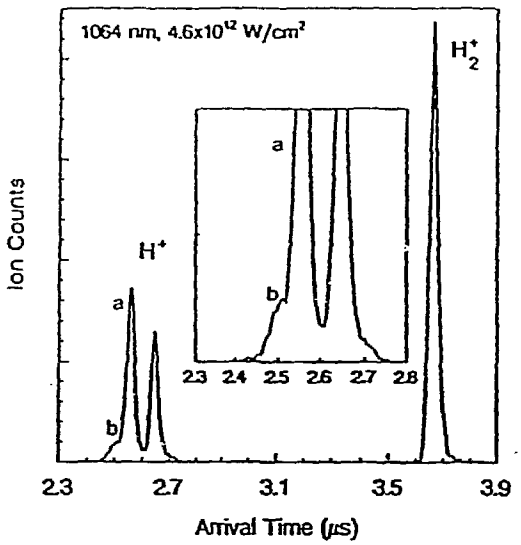

Figure 3: Time-of-flight mass spectrum of H_2 resulting from 1.06 μm excitation at an intensity of 4.6 x 10^{12} W/cm^2. The peak labelled H_2^+ at 3.7 μs results from the MPI of H_2. The protron peaks labelled *a* and *b* are the forward velocity components formed via the 2- and 4- photon dissociation of H_2^+. The insert is an expanded view of the proton distribution.

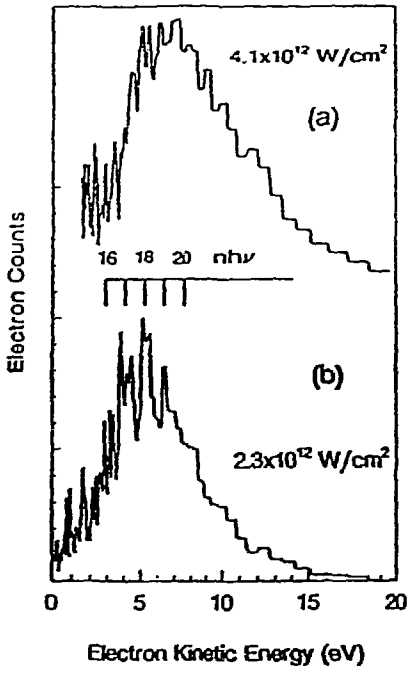

Figure 4: Photoelectron spectrum of H_2 molecule taken at different laser intensities with 1.06 μm radiation. The tick marks indicate the number of absorbed photons above the H_2 ground state.

DiMauro

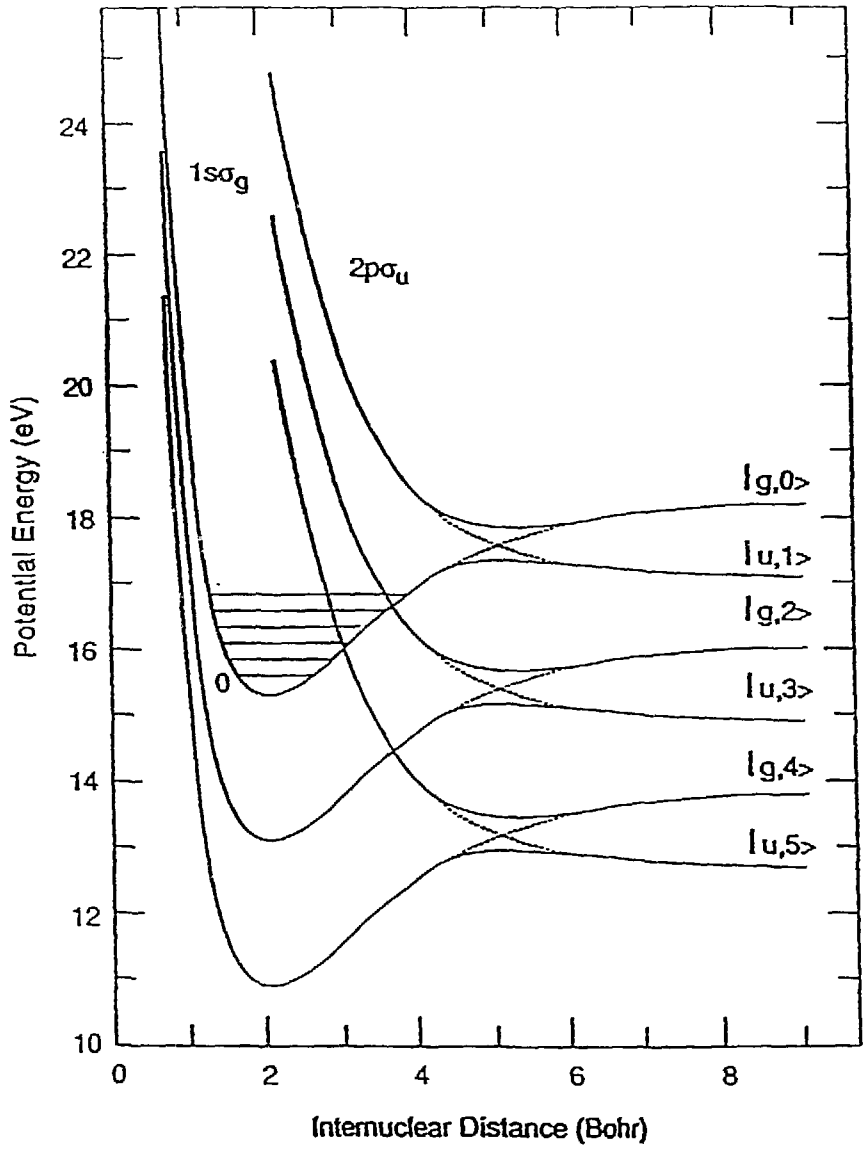

Figure 5: The dressed-state H_2^+ molecular potentials for a 1.06 μm field. The dressed-state $|s, N>$ notation is as follows; s equals the diabatic molecule potential (where g= $^2\Sigma_g^+$ [1sσ_g] and u= $^2\Sigma_u^+$ [2pσ_u]) and N is the photon number. The dotted lines shows the diabatic crossing which distorts (full lines) due to the molecule-field interaction. The avoid-crossings at 3.6 and 3.1 bohr represent the 3 and 5-photon absorptions.

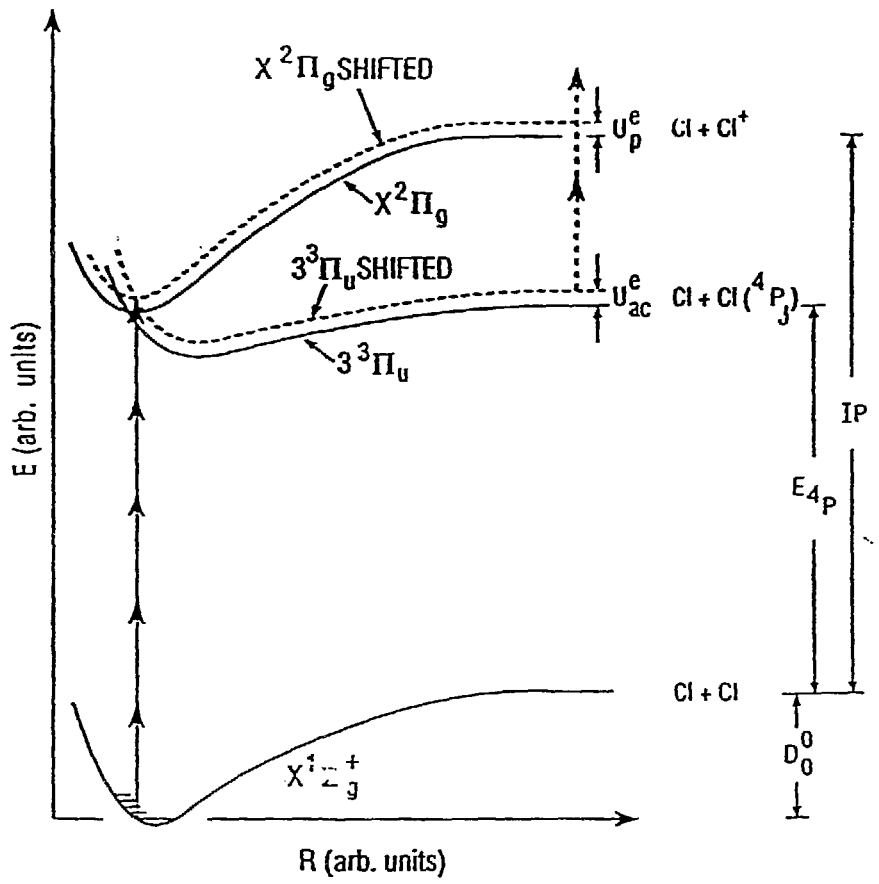

Figure 6: Some relevant potential energy curves for chlorine molecule and their dissociative limits. The terms labelled are those relevant to equations in text. The dashed lines are the field-shifted potential curves. For simplicity, the ac-Stark shift is shown independent of internuclear distance but the field shifts could be R dependent.

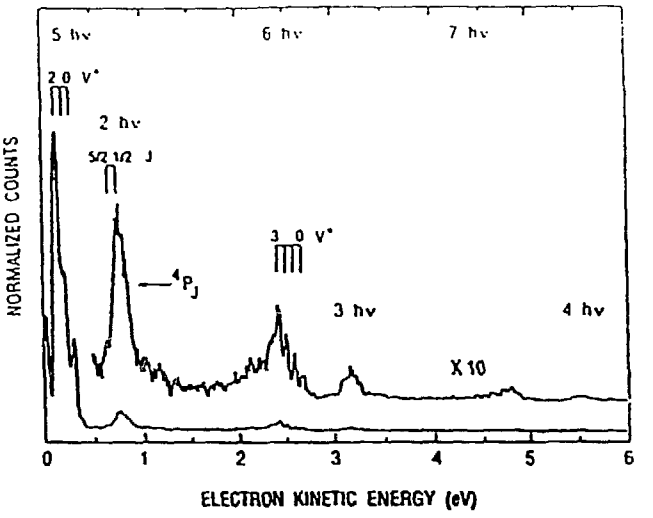

Figure 7: Photoelectron spectrum of chlorine with 0.53 μm radiation at 3×10^{12} W/cm^2. The tick marks above the ^4P_J peak show expected electron energy peaks from the unperturbed J levels while the molecular peaks show the different unperturbed vibrational states of the Cl_2^+ ground state.

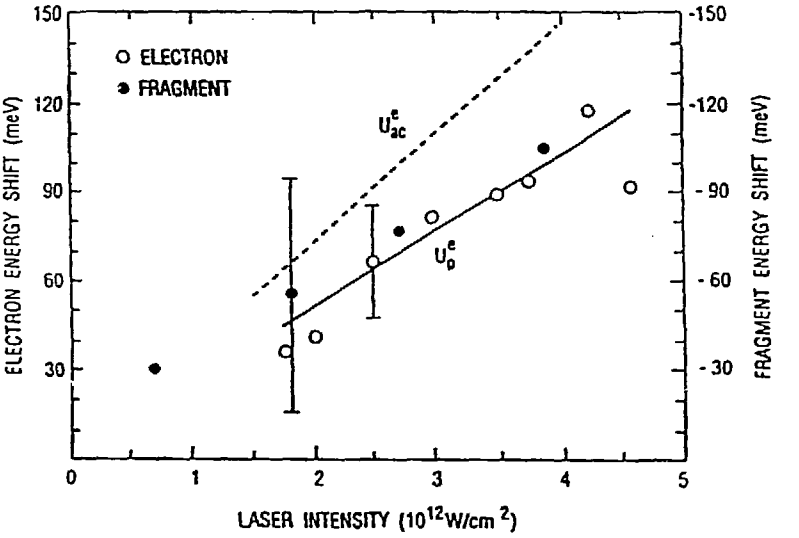

Figure 8. Photoelectron (open circles) and ^4P chlorine fragment (solid circles) kinetic energy shifts as a function of 0.527 μm laser intensity. The typical error associated with the electron and mass spectrometer measurements are shown by the vertical bars. The dashed line shows the calculated SQDT ac-Stark shift of the Cl atom's ^4P state. The solid line results assuming a pure (free-electron) ponderomotive shift and provides a line of reference for the reader.